Soriano, A., Navarro, E., Paul, D. L., Porti, J. A., Morente, J. A., & Craddock, I. J. (2005). Finite difference time domain simulation of the Earth-ionosphere resonant cavity: Schumann resonances. IEEE Transactions on Antennas and Propagation, 53(4), 1535 - 1541. [Issue 4]. 10.1109/TAP.2005.844415

Finite Difference Time Domain Simulation of the Earth-Ionosphere Resonant Cavity: Schumann Resonances

Antonio Soriano, Enrique A. Navarro, Dominique L. Paul, Jorge A. Portí, Juan A. Morente, and Ian J. Craddock

***Abstract*—This paper presents a numerical approach to study the electrical properties of the Earth's atmosphere. The finite-difference time-domain (FDTD) technique is applied to model the Earth's atmosphere in order to determine Schumann resonant frequencies of the Earth. Three-dimensional spherical coordinates are employed and the conductivity profile of the atmosphere versus height is introduced. Periodic boundary conditions are implemented in order to exploit the symmetry in rotation of the Earth and decrease computational requirements dramatically. For the first time, very accurate FDTD results are obtained, not only for the fundamental mode but also for higher order modes of Schumann resonances. The proposed method constitutes a useful tool to obtain Schumann resonant frequencies, therefore to validate electrical models for the terrestrial atmosphere, or atmospheres of other celestial bodies.**

***Index Terms*—Earth-ionosphere waveguide, extremely low frequency (ELF), finite-difference time-domain (FDTD) methods, propagation.**

I. Introduction

THE ionosphere and Earth's surface could be considered like conductors, both of them delimiting an enormous resonant cavity. Resonant frequencies associated with this cavity are in the Extremely Low Frequency (ELF) range because of the Earth dimensions. These eigenfrequencies, also called Schumann frequencies, were predicted by W. O. Schumann in 1952 [1], and detected by Balser and Wagner in 1960 [2]. Schumann resonance frequencies are related to several geophysical phenomena like earthquakes and lightning. Nowadays, the interest in Schumann resonances has increased considerably mainly due to the following.

- The existence of a clear correlation between Schumann frequencies and the tropical temperature [3].
- The relationship between Schumann frequencies and lightning which permits the exploration of terrestrial-like electrical activity in other celestial bodies such as Mars [4] and the Saturnian moon, Titan [5].

Manuscript received April 8, 2004; revised July 19, 2004. This work was supported by Spanish government projects TIC2002-04096-C03-01, FIS2004-03273, and under Grant AP2001-3741.

A. Soriano, J. A. Portí, and J. A. Morente are with the Department of Applied Physics, University of Granada, 18071-Granada, Spain.

E. A. Navarro is with the Department of Applied Physics, University of Valencia, 46100 Valencia, Spain (e-mail: enrique.navarro@uv.es).

D. L. Paul and I. J. Craddock are with the Department of Electrical and Electronic Engineering, University of Bristol, BS8 1UB Bristol, U.K. (e-mail: d.l.paul@bristol.ac.uk).

Digital Object Identifier 10.1109/TAP.2005.844415

Techniques available in the literature for the study of Schumann resonances are primarily based upon frequency-domain waveguide theory [6]. Recently, Cummer [7] applied a two-dimensional (2-D) finite-difference time-domain (FDTD) technique in cylindrical coordinates to the modeling of propagation from lightning radiation in the Earth-ionosphere waveguide. Cummer showed that the FDTD technique was extremely well suited to the characterization of such a phenomenon in very low frequency (VLF) range. In a more recent paper, Simpson and Taflove [8] developed a two-dimensional FDTD technique involving a mix of trapezoidal and triangular cells to map the entire surface of the Earth and described antipodal ELF propagation and Schumann resonances. Although Simpson and Taflove achieved very good accuracy for the fundamental Schumann resonance, their two-dimensional model excluded the characterization of higher order Schumann resonances.

In this paper, an electrical model of the Earth's atmosphere based on FDTD technique is presented, which permits the characterization of Schumann resonances. To model the Earth-ionosphere cavity, a three dimensional mesh in spherical coordinates is employed. Computational demands are minimized by the implementation of periodic boundary conditions. A simple model of the atmosphere considers the Earth's surface and the ionosphere as perfect conductors, the gap between both conducting surfaces being around 60 Km. This model provides a first approximation to derive Schumann resonances, but better results are obtained when electrical conductivity is inserted into the model. An accurate model which includes the conductivity profile of the atmosphere versus height is presented, where the Earth's surface acts as a perfect conductor and the ionosphere like a good, but imperfect conductor. In the second model, the gap between the Earth's surface and the ionosphere is around 100 Km, and the conductivity profile is obtained from [9], and [10].

Our model does not include ionosphere day/night asymmetry, neither the anisotropy of the ionosphere or the magnetic field. We look for resonant frequencies below 50 Hz in the Earth. Because of the spherical symmetry, the resonant frequencies have no dependence in ϕ, [10], then in our model we assume there is no ϕ variation for all the field values, deriving in a 2-D azimuthally symmetry. However our FDTD scheme is three dimensional, we can introduce more cells along the ϕ direction to complete the Earth for a future analysis of day/night ionosphere asymmetry.

We demonstrated that a simple numerical model can produce accurate results. This is a very simple model also efficient in

terms of computer resources. So far, no other equivalent numerical technique FDTD or TLM achieves the accuracy of our model.

II. Numerical Model

A. FDTD Technique in Spherical Coordinates

The FDTD technique usually uses a rectangular coordinate system because of its simplicity. When the geometry of the problem under study does not align with the axes of the rectangular coordinate system, nonorthogonal techniques are usually employed to avoid the staircasing effect [11], [12]. Cylindrical or spherical coordinate systems are hardly ever used in FDTD modeling. Since the Earth has an almost spherical symmetry, the spherical coordinate system is especially suitable to model the Earth-ionosphere cavity. This choice of the coordinate system is useful for the reduction of computing resources such as memory and computation time.

The use of curvilinear coordinates is described by Fusco in [13]. Curvilinear systems require the use of the integral expressions of the Maxwell curl equations in free source regions

$$-\mu \int_S \frac{\partial \overrightarrow{H}}{\partial t} d\overrightarrow{s} = \oint_L \overrightarrow{E}\, d\overrightarrow{l} \tag{1a}$$

$$\epsilon \int_S \frac{\partial \overrightarrow{E}}{\partial t} d\overrightarrow{s} = \oint_L \overrightarrow{H}\, d\overrightarrow{l}. \tag{1b}$$

In the above equations, S represents the integration surface, and L is a closed integration path which delimits the surface S.

The continuous electric and magnetic fields are discretized to obtain the FDTD equations. The discretization of the radial component of the electric field is

$$\begin{aligned} E_r(\overrightarrow{r}, t) &\approx E_r(R_T + (i+0.5)\triangle r, j\triangle\theta, k\triangle\phi, n\triangle t) \\ &= E_r^n(i,j,k) \end{aligned} \tag{2}$$

where the parameter R_T is the Earth's radius, and i, j and k are integers corresponding to the r, θ and ϕ directions, respectively.

The explicit inclusion of the Earth's radius into the FDTD updating equations in spherical coordinates avoids the modeling of inner points where no propagation occurs. By only modeling the Earth's atmosphere the mesh size is reduced considerably. Discrete equations are obtained taking into account the position of the electric and magnetic field components in the spherical nodes, as illustrated in Figs. 1 and 2

$$\begin{aligned} H_r^{n+(1/2)}(i,j,k) = H_r^{n-(1/2)}(i,j,k) + \frac{\triangle t}{\mu S_{hr}(i,j)} \\ \times \Big\{ \big[E_\phi^n(i,j,k)\cdot l_{e\phi}(i,j) \\ - E_\phi^n(i,j+1,k)\cdot l_{e\phi}(i,j+1)\big] \\ - \big[E_\theta^n(i,j,k)\cdot l_{e\theta}(i) \\ - E_\theta^n(i,j,k+1)\cdot l_{e\theta}(i)\big] \Big\}. \end{aligned} \tag{3}$$

The magnetic field component in the radial direction is updated with the above equation at each $n+1/2$ time step. Similar expressions are derived to update the electric field and the other magnetic field components. The coefficient S_{hr} in (3) represents

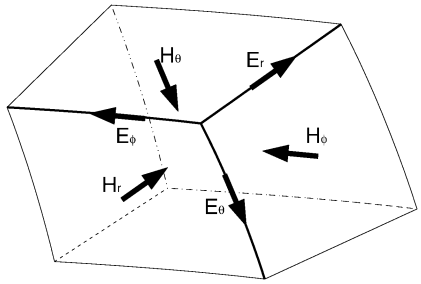

Fig. 1. FDTD node in spherical coordinates.

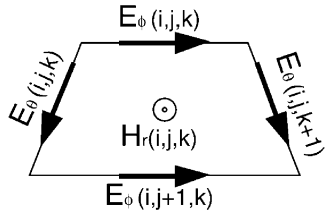

Fig. 2. FDTD-grid normal to the radial component in the northern hemisphere.

the integration surface element corresponding to each cell, it is obtained by integrating the differential surface element in the radial direction dS_r. Similar coefficients are evaluated in the θ and ϕ directions, (4)

$$\begin{aligned} S_{hr}(i,j) &= \int_{k\triangle\phi}^{(k+1)\triangle\phi} d\phi \int_{j\triangle\theta}^{(j+1)\triangle\theta} r^2 sin(\theta) d\theta \\ &= (R_T + i\triangle r)^2 \\ &\quad \triangle\phi\{\cos(j\triangle\theta) - \cos((j+1)\triangle\theta)\} \end{aligned} \tag{4a}$$

$$\begin{aligned} S_{h\theta}(i,j) &= \int_{k\triangle\phi}^{(k+1)\triangle\phi} d\phi \int_{i\triangle r}^{(i+1)\triangle r} r\sin(\theta) dr \\ &= (R_T + (i+0.5)\triangle r) \\ &\quad \cdot \sin((j+0.5)\triangle\theta)\triangle r\triangle\phi \end{aligned} \tag{4b}$$

$$\begin{aligned} S_{h\phi}(i) &= \int_{j\triangle\theta}^{(j+1)\triangle\theta} d\theta \int_{i\triangle r}^{(i+1)\triangle r} r dr \\ &= (R_T + (i+0.5)\triangle r)\triangle r\triangle\theta. \end{aligned} \tag{4c}$$

The coefficients $l_{e\theta}$ and $l_{e\phi}$ in (3) correspond to the length of the integration path in each direction, and describe the geometrical properties of the mesh in the spherical coordinate system. As in the previous case regarding surface parameters, these coefficients are evaluated by integrating the differential length elements along the cell edges

$$l_{er} = \triangle r \tag{5a}$$

$$l_{e\theta}(i) = (R_T + i\triangle r)\triangle\theta \tag{5b}$$

$$l_{e\phi}(i,j) = (R_T + i\triangle r)\sin(j\triangle\theta)\triangle\phi. \tag{5c}$$

These coefficients are position-dependent, hence, their expressions include the position indexes. However, some of them, because of our discretization, have constant values, or depend on one or two indexes.

B. Handling of the Discontinuities in the System

Two important discontinuities exist in the spherical coordinate system [13]. The first one is placed at the origin of the co-

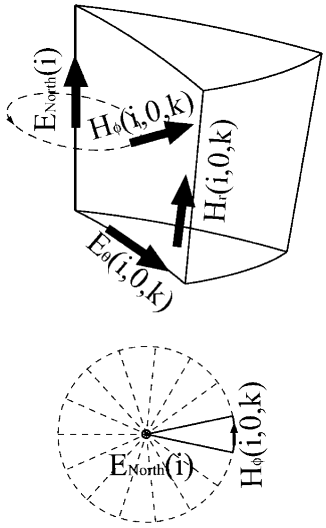

Fig. 3. Detail of the north pole discontinuity.

ordinate system, the other one is along the north-south (N-S) axis. As our numerical mesh does not include the origin the first discontinuity needs not to be addressed. Therefore, attention is given to the zenithal angles $\theta = 0$ and $\theta = \pi$, (N-S axis). To overcome this discontinuity, a suitable choice of the field distribution is needed. As shown in Fig. 3, an alternative circular path for the H_ϕ, surrounding the discontinuity in the N-S axis, is used to update E_r. The following integral equation was solved to update E_r along the discontinuity:

$$\epsilon \int_0^{2\pi} d\phi \int_0^{((\triangle\theta)/2)} \frac{\partial E_r(r,\theta,\phi,t)}{\partial t} r^2 \sin(\theta) d\theta = \oint_0^{2\pi} H_\phi \left(r, \frac{\triangle\theta}{2}, \phi, t\right) r \sin\left(\frac{\triangle\theta}{2}\right) d\phi. \quad (6)$$

We introduce the special points $E^n_{\mathrm{North}}(i)$ and $E^n_{\mathrm{South}}(i)$. $E^n_{\mathrm{North}}(i)$ represents the electric field along the N-S axis in the northern hemisphere ($\theta = 0$), and $E^n_{\mathrm{South}}(i)$ corresponds to the southern hemisphere ($\theta = \pi$). In the following we develop the updating equations for $E^n_{\mathrm{North}}(i)$, analogous equations are derived for $E^n_{\mathrm{South}}(i)$.

$$\int_0^{2\pi} d\phi \int_0^{\triangle\theta/2} \frac{\partial E_r(r,\theta,\phi,t)}{\partial t} r^2 \sin(\theta) d\theta \approx \left\{E^{n+1}_{\mathrm{North}}(i) - E^n_{\mathrm{North}}(i)\right\} S_{er}(i,0). \quad (7)$$

The $S_{er}(i,0)$ coefficients represent a circular surface, shown in the bottom of Fig. 3, enclosed by a circular path along the middle of the sectoral cells that are shown in the top of Fig. 3. Then, $S_{er}(i,0)$ are obtained by adding the surface of each circular sector of angle $\triangle\phi$. The discretization along the ϕ axis is $k_{\max}$, then each sectoral cell has $\triangle\phi = 2\pi/k_{\max}$.

Equations (6) and (7) will provide the updating equation for $E^n_{\mathrm{North}}(i)$ using the H_ϕ components that belong to the special sectoral cells located around the N-S axis, top of Fig. 3. The numerical integration of the right side of (6) reduces to a sum for the H_ϕ components along the circular path of Fig. 3. Each $H^{n+0.5}_\phi(i,0,k)$ component in the circular path corresponds to

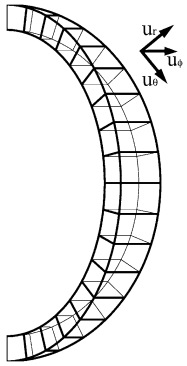

Fig. 4. FDTD grid used to compute Schumann resonances.

a distinct sectoral k-cell that surrounds the N-S axis. Thus, the final updating equation for the E_{North} points is

$$E^{n+1}_{\mathrm{North}}(i) = E^n_{\mathrm{North}}(i) + A_i \sum_{k=0}^{k_{\max}} H^{n+0.5}_\phi(i,0,k). \quad (8)$$

The coefficient A_i, introduced in (8), depends on the discretization and electrical properties. It includes all geometrical and electrical coefficients involved in the updating equation for the electrical field along the N-S axis

$$A_i = \frac{l_{h\phi}(i,0)\triangle t}{\epsilon S_{er}(i,0)} = \frac{\triangle t \triangle\phi}{2\pi\epsilon[1-\cos(0.5\triangle\theta)](R_T + (i+0.5)\triangle r)}. \quad (9)$$

Analogous equations are derived for the E^n_{South} special points.

C. Reduction of Modeling Requirements

Although a three dimensional model is required to simulate the entire atmosphere, it is possible to reduce significantly the computational cost required to obtain resonant frequencies of the Earth-ionosphere cavity. This is possible because of the degeneracy of the expected solution in spherical coordinates along the ϕ direction, see [10]. By using this property, a simpler mesh with only one cell along the ϕ direction, but still containing three dimensional information, is strictly required to obtain Schumann resonances. The mesh used to obtain Schumann resonances is shown in Fig. 4. Also, periodic boundary conditions are implemented to consider that electric and magnetic fields are ϕ independent. The following equations enforce the periodic boundary conditions for the radial components:

$$E_r(i,j,2) = E_r(i,j,1)$$
$$H_r(i,j,0) = H_r(i,j,1). \quad (10)$$

The complete implementation of the periodic boundary conditions requires analogous expressions for the θ components of the electric and magnetic fields. These conditions are introduced to enforce no-field variations along the ϕ direction. Therefore, our model reduces the mesh to a single cell along ϕ-axis.

In addition to periodic boundary conditions, a special treatment of the $\theta = 0, \pi$ axis is required to reduce the (6)–(9) to

consider a single cell along ϕ direction. As mentioned before, in order to reduce computational requirements no variation of the electromagnetic field is assumed along the ϕ axis. Thus, $H_\phi(i,0,k)$ remains constant along the ϕ direction (k-index). Then the updating equation for $E^n_{\rm North}(i)$ in this particular symmetry is

$$E^{n+1}_{\rm North}(i) = E^n_{\rm North}(i) + \frac{\triangle t}{\epsilon[1-\cos(0.5\triangle\theta)][R_T+(i+0.5)\triangle r]} \cdot H^{n+0.5}_\phi(i,0,k). \quad (11)$$

Although the numerical model is three dimensional, because of the ϕ-symmetry, our simulation is carried out for a single cell along the ϕ direction. But a closed circular integration path is required to update the electric field at the N-S axis. The (8) is evaluated takeing into account the periodic boundary conditions, this implies that H_ϕ has symmetry along the ϕ *axis*. Thus, the sum in (8) is $(2\pi/\triangle\phi)$ times greater the magnetic field evaluated at the computed cell.

D. Treatment of Losses

When losses are present, the Maxwell equations are modified to include Joule effect. Losses in a real conducting media are introduced by means of a finite conductivity σ, that in our model for the ionosphere are dependent on the radial distance to the Earth surface, $\sigma = \sigma(r)$. The profile for the ionosphere conductivity for our numerical model was obtained from [9] and [10]

$$-\mu \int_S \frac{\partial \overrightarrow{H}}{\partial t} d\overrightarrow{s} = \oint_L \overrightarrow{E}\, d\overrightarrow{l} \quad (12a)$$

$$\epsilon \int_S \frac{\partial \overrightarrow{E}}{\partial t} d\overrightarrow{s} + \int_S \sigma(r)\overrightarrow{E}\, d\overrightarrow{s} = \oint_L \overrightarrow{H}\, d\overrightarrow{l}. \quad (12b)$$

The discretization of the above equations is carried out following a similar treatment as in previous sections. However the linear temporal differentiation is replaced by a first order exponential scheme, that can be found in [14] and is more appropriated when high losses are present. The first order exponential scheme is well suited for the modeling of layered structures with high losses using a reduced number of cells, providing more accurate results than other linear schemes.

The discrete updating equation for E_r when considering losses is

$$E^{n+1}_r(i,j,k) = e^{-((\sigma(i)\triangle t)/\epsilon)} E^n_r(i,j,k) + \frac{1-e^{-((\sigma(i)\triangle t)/\epsilon)}}{\sigma(i) S_{er}(i,j)} \times \left\{ \left[H^{n+(1/2)}_\phi(i,j,k)\cdot l_{h\phi}(i,j) - H^{n+(1/2)}_\phi(i,j-1,k)\cdot l_{h\phi}(i,j-1) \right] - \left[H^{n+(1/2)}_\theta(i,j,k)\cdot l_{h\theta}(i) - H^{n+(1/2)}_\theta(i,j,k-1)\cdot l_{h\theta}(i) \right] \right\}. \quad (13)$$

where the conductivity in ionosphere is stratified, $\sigma = \sigma(r)$.

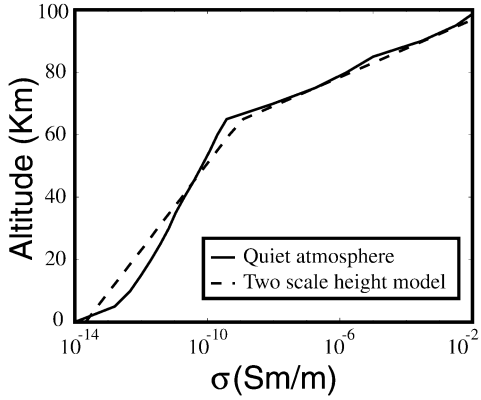

Fig. 5. Conductivity profile of the terrestrial atmosphere.

Similar equations to (13) are obtained for the rest of electric field components, whereas the updating equations for the magnetic field components are the same for both lossless and lossy cavity because Faraday's Law does not change when introducing losses, see (1a) and (12a).

III. Numerical Results

The utility of the proposed technique is the numerical calculation of Schumann resonances of any celestial body, with a given radius and atmosphere conductivity profile. To verify the utility of the technique, a model for the Earth is built. In this model, the atmosphere is assumed to be a vacuum medium bounded by perfect conductors. The inner conductor is the Earth surface, and the outer one is assumed the be located at the lower layer of the ionosphere. The analytical solution for the electromagnetic field in a region bounded by two spherical conductors can be found in [10].

The simple lossless model is based in two facts. First, the conductivity of the Earth's surface ranges from 10^{-3} to 10^{-5} S/m at solid parts to 4 S/m at ocean surfaces. These values ensure that the Earth's surface behaves as a good conductor in the ELF range. Second, if we consider Fig. 5 which shows the conductivity profile for a quiet atmosphere surrounding the Earth [10], a considerably higher slope of the conductivity versus altitude is observed for heights above 60 Km. Therefore, an initial simple model for the atmosphere thickness is a 60 Km vacuum region, bounded by two spherical perfect conductor surfaces.

The atmosphere is simulated using a 12×120 mesh, resulting in spatial and angular discretizations of: $\triangle r = 5$ Km and $\triangle\theta = 1.5°$. As mentioned before, only one cell was computed along the ϕ direction, the angular cell size is $\triangle\phi = 9°$. The discretizations along r and θ directions ($\triangle r$ and $\triangle\theta$ respectively) are chosen depending on geometric parameters. The length of the cell along ϕ direction is less important to the results than the other two. The criterion we used to determine this value was a balance to get cells as squared as possible in equator and poles. Because the cell length in the ϕ direction depends on the latitude, l_ϕ is shorter in the poles than in the equator.

The Schumann resonances of the Earth-ionosphere cavity are obtained by performing the fast Fourier transform (FFT) over the time domain fields. Since the Schumann resonances are in the ELF range, a large simulation time $(N\triangle t)$ is required to

TABLE I
THEORETICAL AND NUMERICAL RESONANT FREQUENCIES (IN HERTZ) FOR A 60 KM LOSSLESS ATMOSPHERE. n IS THE INDEX OF THE RESONANCE

n	1	2	3	4	5	6
TLM Resonances	10.50	18.28	25.90	33.51	41.46	49.42
Deviation (%)	0.4	0.1	0.3	0.3	1.6	2.3
FDTD Resonances	**10.49**	**18.20**	**25.91**	**33.41**	**40.90**	**48.18**
Deviation (%)	**0.4**	**0.1**	**0.3**	**0.2**	**0.2**	**0.3**
Theoretical Resonances	10.54	18.26	25.83	33.34	40.83	48.32
Experimental Resonances	7.8	14	20	26	33	39

achieve the desired FFT resolution, given by $\triangle f = (N\triangle t)^{-1}$. The Courant stability criterion restricts the time step to $\triangle t = 1.610^{-5}$ s. Therefore, a large number of time iterations is required in order to achieve sensitivity enough for the FFT. In our simulations, a total of $N = 400\,000$ time steps are necessary to obtain a frequency resolution $\triangle f = 0.16$ Hz.

Table I summarizes the results obtained with the FDTD technique. These are compared against analytical and transmission line matrix (TLM) results for the Earth-ionosphere cavity without losses [10]. Resonant frequencies obtained with the TLM method and FDTD are very similar, the main difference between TLM and FDTD is that the first method uses analogous transmission line circuits whose voltages and currents define the electromagnetic field, while FDTD technique directly evaluates the electromagnetic field by solving Maxwell equations through a finite difference scheme. The similarity of the numerical resonances obtained with both analytical and numerical results serves as validation for the proposed technique. However, there is a significant difference between the numerical results and the measured Schumann resonances.

Once the results provided by the previous simulations validated our FDTD scheme given in Section II, a more accurate model for the terrestrial atmosphere including losses was considered. This model introduces the conductivity profile, obtained from [9] and [10], of the quiet atmosphere shown in Fig. 5. Now, the Earth's surface is modeled as a perfect conductor ($\sigma = \infty$), and the ionosphere layer is modeled like good conductors (profile $\sigma(r) \neq \infty$). Although the losses through the layers of ionosphere are really small (about 10^{-6} parts of the incident wave), they have a considerably influence in the derived numerical frequencies.

In the present model, a 100 Km thick atmosphere layer is simulated. In order to maintain the cell dimensions in the radial direction, the mesh used for this simulation is larger than the one used for the previous one, 20×120 cells are considered. In the radial direction the mesh finishes with five additional cells with perfect matched layers (PML), backed by a perfect conductor. The number of time steps (N), and the frequency resolution are unchanged from the previous model. The mesh has 20 cells per wavelength for the 6th mode. However we also tried finer meshes, in using a mesh with twice the density we did not get a significant improvement, but consumed more computer resources. The mesh is optimal for the frequency band 5–50 Hz, to calculate the Schumann frequencies up to 50 Hz. Our program runs in a Pentium IV personal computer with

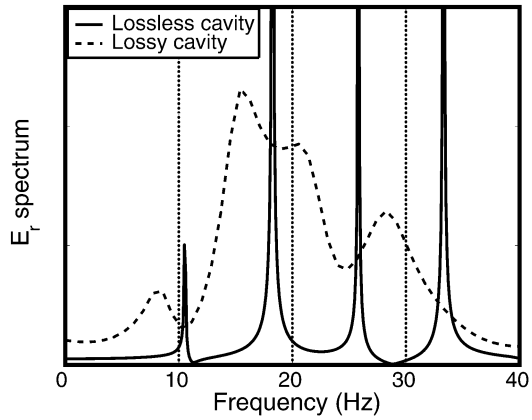

Fig. 6. Spectral response at equator points.

512 Mb RAM, it takes around 10 minutes per simulation. The E_r spectral response of the Earth-ionosphere cavity is obtained by doing the FFT of the time domain fields, it is presented in Fig. 6 for both lossless and lossy cavities. The sharpest resonance peaks correspond to the lossless cavity, while a quasi-continuum-soft spectrum is obtained with the model including the conductivity profile. This is because of the overlapping of contiguous modes, caused by the broadening of the resonant response after the introduction of losses. This spectral response is typical from a low Q structure, where losses are present. To estimate the resonant frequencies two different approaches are used. The first is a perturbation approach, were the lossless modes obtained from the first model are used to excite the ionosphere with losses: Two sets of modes, with spaced frequencies provide sharp and spaced peaks with the FFT. In that way, two simulations were used, the first for 1–3–5 modes, and the second for 2–4–6 modes. The second approach uses the multiple signal classification (MUSIC) libraries of MATLAB,[1] and a single time series from the time domain fields. Results using both approaches present negligible differences.

To compare our numerical results with other existing ones, let us consider a semi-analytical model based on the qualitative behavior of the Earth's quiet atmosphere conductivity shown in Fig. 5. Two different regions with a common interface at around 60 Km altitude are clearly appreciated in this figure. Approximately, region I corresponds to heights below 60 Km height and region II for heights above 60 Km. The conductivity increases with height in both regions, but the increase is faster in the external region. This dual behavior is the basis of the two-scale height ionospheric model proposed by Sentman in 1990 [15], which is widely accepted by the scientific community working on Schumann resonances. The model uses the following approximate conductivity profile:

$$\sigma(r) = \begin{cases} \sigma_1 e^{((r-h_1)/\xi_1)}, & \text{(region I)} \\ \sigma_2 e^{((r-h_2)/\xi_2)}, & \text{(region II)} \end{cases} \tag{14}$$

where stands for the altitude above ground level, ξ_1 and ξ_2 are local scale heights which range from 3 to 5 Km, depending on the authors, the termed ELF conducting boundary h_1 is the height where $\sigma_1 = \epsilon_o \omega$, and the ELF reflection boundary h_2

[1]MATLAB is a registered trademark of The MathWorks, Natick,MA.

TABLE II
RESONANT FREQUENCIES (IN HERTZ) AND PERCENTAGE DEVIATION FOR A 100 KM ATMOSPHERE WITH CONDUCTIVITY PROFILE. n IS THE INDEX OF THE RESONANCE

n	1	2	3	4
Two-layer Resonances	7.9	13.7	19.4	25.0
Deviation (%)	1.3	2.1	3.0	3.8
TLM Resonances	8.3	15.8	22.0	29.4
Deviation (%)	6.4	12.8	10.0	13.0
2D FDTD Resonances [8]	7.46	-	-	-
Deviation (%)	4.4	-	-	-
3D FDTD Resonances	**8.1**	**15.4**	**20.6**	**28.3**
Deviation (%)	**3.8**	**10**	**3**	**8.8**
Experimental Resonances	7.8	14	20	26

is the altitude where $4\mu_o\omega\sigma_2\xi_2^2 = 1$. Typical values of these heights range from 40 to 50 Km for h_1, and from 75 to 90 Km for h_2. The conductivity profile of the two-scale ionospheric model matching the experimental conductivity at 45 and 75 Km altitude is also shown in Fig. 5.

Regarding the model details, it assumes that there is no altitude-dependence of the magnetic field in region I and that the transverse-to-r electric field is zero at the Earth's surface and also in the region II. Matching the electric potential at the interface between regions I and II, the two-layer model yields the following eigenfrequencies for the Earth-ionosphere cavity:

$$f_l = \sqrt{l(l+1)}\frac{c}{2\pi a}\left(\frac{h_1 - \frac{\pi}{2}\xi_1}{h_2 + \frac{\pi}{2}\xi_2}\right)^{(1/2)} \tag{15}$$

where $l = 1, 2, \ldots$ is an integer number. Using this expression with typical values $h_1 = 50$ Km, $h_2 = 90$ Km, and $\xi_1 = \xi_2 = 5$ Km, a set of Schumann resonances in good agreement with experimental observations are obtained. These values are also included in Table II showing an excellent agreement with measured data. The main problem with this semi-analytical model is that is only valid for atmospheres whose conductivity profile shows the two-slopes behavior, and even in these cases, the model parameters must be adjusted to that particular case. In other words, the model is not directly exportable to other planetary atmospheres without specific calibration in contrast to the proposed FDTD solution which only requires the inclusion of the conductivity profile and boundaries of the atmosphere under study.

To summarize, despite the different methods used to evaluate Schumann frequencies shown in Table II, the results obtained with our FDTD numerical scheme are in good agreement with the experimental ones, and also with the two-scale height ionospheric model. From our knowledge, summarized in Table II, our FDTD numerical scheme provides the best numerical approach from the 1st to the 4th Schumann resonances, having lower deviation than other existing numerical approximations. Deviation ranges from 3% (third mode) to 10% (second mode), whereas TLM results show deviations ranging from 6.4% (first mode) to 13% (fourth mode). These deviations are associated to the contribution of different parts of the numerical model, the inherent numerical errors of FDTD, and FFT sensitivity. Also it is associated to the model of ionosphere that does not include the differences between day time and night time. It is very difficult to make the separation between all these errors. We believe that the main source of errors is associated to day-night-time changes in ionosphere. Our results are also more accurate than the results presented by Simpson and Taflove for the first mode [8] using a 2-D FDTD scheme. However, the accuracy of the presented scheme is globally overcome by the semi-analytical two-scale height ionospheric model. This semi-analytical method adjusts the conductivity profile to obtain the Schumann resonance frequencies, whereas in numerical methods the conductivity is a given parameter. Then, numerical procedures as our FDTD scheme, either 2-D FDTD or TLM provide a more flexible and also a more general solution.

IV. CONCLUSION

A three-dimensional (3-D) spherical FDTD model of the terrestrial atmosphere was presented in this paper. An important reduction of the computational cost has been achieved considering the symmetries of the problem. For the first time, numerical FDTD frequencies for the first four Schumann resonances are obtained with an acceptable computational cost and a good accuracy.

A lossless FDTD model of the Earth's atmosphere was first developed in order to validate the technique by comparison with existing analytical values [10]. Better accuracy can be achieved when a more complete model including the conductivity profile of the atmosphere and losses at the ionosphere layers is introduced. Results show comparable accuracy to semi-analytical results obtained with the widely accepted two-scale height ionospheric model and better than other numerical results derived from other techniques. Therefore, the proposed FDTD scheme may be considered as a valid procedure to study the electrical properties of the atmosphere of the Earth and other celestial bodies.

ACKNOWLEDGMENT

The authors would like to thank Profs. D. Bull and J. P. McGeehan for provision facilities at the Electrical and Electronic Engineering Department of the University of Bristol, Bristol, U.K.

REFERENCES

[1] W. Schumann, "Über die stralungslosen eigenschwingungen einer leitenden kugel die von luftschicht und einer ionosphärenhülle umgeben ist," *Z. Naturforsch A*, vol. 7, pp. 149–154, 1952.

[2] M. Balser and C. Wagner, "Observations of earth-ionosphere cavity resonances," *Nature*, vol. 188, pp. 638–641, 1960.

[3] E. Williams, "The Schumann resonance: A global tropical thermometer," *Sci.*, vol. 256, pp. 1184–1187, 1992.

[4] K. Schwingenschuch, G. Molina-Cuberos, W. Magnes, M. Menvielle, M. Friedrich, and P. Falkner, "Low frequency electromagnetic waves near the Martian surface," in *Proc. 2nd NetLander Scientific Workshop*, Nantes, France, 2001.

[5] M. Fulchignoni *et al.*, "The Hyugens atmospheric structure instrument (HASI)," *European Space Agency Scientific Publications*, vol. 1177, pp. 163–176, 1997.

[6] J. R. Wait, *Electromagnetic Waves in Stratified Media*, 2nd ed, U.K.: Pergamon, 1970.

[7] S. Cummer, "Modeling electromagnetic propagation in the earth-ionosphere waveguide," *IEEE Trans. Antennas Propag.*, vol. 49, no. 9, pp. 1420–1429, Sep. 2000.
[8] J. Simpson and A. Taflove, "Two-dimensional FDTD model of antipodal ELF propagation and Schumann resonance of the earth," *IEEE Antennas Wireless Propag. Lett.*, vol. 1, pp. 53–56, 2002.
[9] K. Schlegel and M. Füllekrug, "Schumann resonance parameter changes during high-energy particle precipitation," *J. Geophys. Res.*, vol. 104, no. A5, pp. 10 111–10 118, 1999.
[10] J. Morente, J. Molina-Cuberos, J. Portí, B. Besser, A. Salinas, K. Schwingenschuch, and H. Litchengger, "A numerical simulation of earth's electromagnetic cavity with the transmission line matrix method: Schumann resonances," *J. Geophys. Res.*, vol. 108, no. A5, 2003.
[11] E. A. Navarro, C. Wu, P. Chung, and J. Litva, "Sensitivity analysis of nonorthogonal FDTD method applied to the study of square coaxial waveguide structures," *Microwave Opt. Technol. Lett.*, vol. 8, pp. 138–140, Feb. 1995.
[12] E. A. Navarro, J. Segura, A. Soriano, and V. Such, "Modeling of thin curved sheets with the curvilinear FDTD," *IEEE Trans. Antennas Propag.*, vol. 52, no. 1, pp. 342–346, Jan. 2004.
[13] M. Fusco, M. Smith, and W. Lawrence, "A three-dimensional FDTD algorithm in curvilinear coordinates," *IEEE Trans. Antennas Propag.*, vol. 39, no. 10, pp. 1463–1471, Oct. 1991.
[14] R. Holland, L. Simpson, and K. Kunz, "Finite-difference analysis of EMP coupling to lossy dielectric structures," *IEEE Trans. Electromagn. Compat.*, vol. EMC-22, pp. 203–209, Aug. 1980.
[15] D. Sentman, "Approximate Schumann resonance parameters for two-scale height ionosphere," *J. Atmospheric Terrestrial Phys.*, vol. 52, no. 1, pp. 35–46, 1990.

Antonio Soriano was born in Benaguasil (Valencia), Spain, in 1978. He received the Licenciado degree in physics from the University of Valencia, Valencia, Spain, in 2001. He has been a Ph.D. student in the University of Granada, Granada, Spain, since 2002.

His research interest is focused on numerical modeling of electromagnetic wave-propagation using the FDTD technique.

Enrique A. Navarro was born in Sueca, Spain, in 1965. He received the Licenciado and the Ph.D. degrees in physics from the University of Valencia, Valencia, Spain, in 1988 and 1992, respectively.

From 1988 to 1989, he was with Grupo de Mecánica del Vuelo S.A. (GMV S.A.), Madrid, Spain. He joined the Department of Applied Physics at the University of Valencia, in 1989 where he is presently a Professor. In 1994 and 1995, he was with the Communications Research Laboratory, McMaster University, Canada. His current research interests include all aspects of numerical methods in electromagnetics, antennas and propagation.

Dr. Navarro was the recipient of a 1993 NATO Fellowship.

Dominique L. Paul received the D.E.A. degree in electronics from Brest University, Brest, France, in June 1986 and the Ph.D. degree from Ecole Nationale Superieure des Telecommunications de Bretagne, Brest, France, in January 1990.

From 1990 to 1994, she was a Research Associate at the Centre for Communications Research, University of Bristol, Bristol, U.K. During 1995 to 1996, she worked as a Research Associate at the Escuela Tecnica Superior de Ingenieros de Telecomunicacion of Madrid, Madrid, Spain under a grant from the Spanish Government. Since 1997, she has been a Research Fellow in the Centre for Communications Research, University of Bristol, with a permanent position since 2003. She has published over 20 papers in conferences and refereed journals. Her research interests include the electromagnetic modeling of passive devices such as microwave heating systems, dielectric structures at millimeter wavelengths, low profile antennas and conformal antenna arrays.

Dr. Paul is a Member of IEEE Antennas and Propagation Society and IEEE Microwave Theory and Techniques Society.

Jorge A. Portí was born in Cartagena, Spain, in 1968. He received the Licenciado in Physics degree and the Ph.D. degree from the University of Granada, Granada, Spain, in 1986 and 1994, respectively.

In 1990, he joined the Applied Physics Department at the University of Granada where he is now a Professor. His research interest is focussed on the numerical modeling of electromagnetic and acoustic wave-propagation phenomena using the transmission line modeling method. His contributions are concerned with the method fundamentals and also with particular electromagnetic applications. He is currently working in the modeling of electromagnetic propagation through planetary atmospheres and through media with time-varying properties.

Juan A. Morente was born in Porcuna (Jaén), Spain, in 1955. He received the Licenciado and Doctor degrees in Physics from the University of Granada, Granada, Spain, in 1980 and 1985, respectively.

He is presently "Profesor Titular" in the Department of Applied Physics at the University of Granada. His main fields of interest include electromagnetic theory and applied mathematics. His current research activities deal with analytical and numerical methods especially for transient electromagnetic fields in planetary atmospheres and for electromagnetic characterization of complex media.

Ian J. Craddock is a Reader in the Centre for Communications Research (CCR), Department of Electrical and Electronic Engineering, University of Bristol, Bristol, U.K. He has active research interests in wideband antenna design, antenna arrays, MIMO, electromagnetic analysis and microwave radar for breast cancer detection. He is part of the EU Framework 6 Antennas Network of Excellence, where he leads a work-package on antennas for GPR, and is a U.K. representative on COST action 284 (Innovative Antennas for Emerging Terrestrial & Space-based Applications).